Relationship between particle deposit characteristics and the mechanism of particle arrival

Daniel Rodríguez-Pérez, Jose L. Castillo, and J. Carlos Antoranz
Departamento de Fisica Matematica y Fluidos, Universidad Nacional de Educacion a Distancia (UNED), Madrid, 28040, Spain
(Received 30 July 2004; revised manuscript received 2 June 2005; published 5 August 2005)

An on-lattice Monte Carlo model is implemented for the simulation of particle deposit growth by advection and diffusion towards a flat surface. The particle deposit structure is characterized by its bulk (density) and interface (mean height and surface width) properties. Numerical correlations, fitted by simple expressions, are reported for these magnitudes, relating them to time (number of deposited particles) and Peclet number. Also a heuristic argument is presented which relates deposit density to local diffusion-limited-aggregation-like processes and interfacial dynamics to the KPZ model.

DOI: 10.1103/PhysRevE.72.021403 PACS number(s): 61.43.Hv, 61.43.Bn, 61.43.Gt

I. INTRODUCTION

In particle-laden gas streams, the particles suspended in the gas can be driven towards neighboring walls by different mechanisms such as inertia, convection, diffusion, and gravitational or phoretic forces, leading to the formation of particle deposits on these surfaces exposed to the stream. In the range of very small particles, inertia plays no role and the particle motion can be split into two contributions [1–4]. A deterministic mean particle velocity is associated with convection (the velocity of the surrounding gas) as well as to the existence of external forces—for instance, buoyancy, thermophoresis, or photophoresis. Moreover, there is a second contribution linked to the particle Brownian motion. This motion corresponds to a random walk of the particle which, averaged (over the ensemble of particles at each location in the gas), is the cause of the Brownian diffusion flux. In the vicinity of the surfaces exposed to the gas, this combination of deterministic motions and/or random walk may take the particles to the surface, leading to the formation of particle deposits. The aim of this work is to relate the deposit mean morphological features to the mechanism of particle arrival to the deposit [5,6]: indeed, to the relative importance of the deterministic particle motion (mean particle velocity) to the random (Brownian) particle walk. Thus, the deposit properties will be analyzed as a function of the Peclet number which measures the relative importance of these two mechanisms.

In the absence of inertia, particles in a gas reach a mean terminal velocity $\mathbf{V}$ corresponding to the balance of forces on them (viscous drag and external-phoretic forces). This velocity together with the Brownian motion characterized by a diffusion coefficient $\mathcal{D}$ gives the following expression for the particle number flux density $\mathbf{j}_c$:

$$\mathbf{j}_c = \mathbf{V}c - \mathcal{D}\,\boldsymbol{\nabla}\, c,$$

where $c(\mathbf{x},t)$ is the number of particles per unit volume at position $\mathbf{x}$ and time t.

Applying the conservation equation for the particles and assuming that both the phoretic force and the diffusion constant $\mathcal{D}$ remain constant within the region of interest, the following evolution equation is obtained:

$$\frac{\partial c}{\partial t} + (\mathbf{V}\cdot\boldsymbol{\nabla})c - \mathcal{D}\nabla^2 c = 0. \tag{1}$$

We will restrict the analysis to the particle behavior in the very vicinity of the walls where the terminal velocity reaches a limiting constant value. There, rescaling the distances with a characteristic length a and expressing the time in units of $\tau = a/V$ (where $V=|\mathbf{V}|$ is the characteristic particle velocity), Eq. (1) becomes

$$Pe\left(\frac{\partial}{\partial t} + \hat{\mathbf{V}}\cdot\boldsymbol{\nabla}\right)c - \nabla^2 c = 0, \tag{2}$$

where $\hat{\mathbf{V}}$ is the unit vector along the direction of $\mathbf{V}$ and Pe stands for the Peclet number,

$$\mathrm{Pe} = \frac{Va}{\mathcal{D}}. \tag{3}$$

Therefore, Pe measures the relative importance of the deterministic particle motion to the nondeterministic particle random walk. Equation (2) for the particle number density corresponds to the Fokker-Plank equation for an ensemble of particles moving in a stochastic manner, assuming dilute conditions—i.e., lack of interaction (e.g., hydrodynamic) among them.

It is well known that in the limit case of $\mathrm{Pe}\to 0$ (purely diffusive particle motion in the absence of drift) the generated particle deposits grow with the fractal structure of the diffusion-limited aggregation (DLA) model [7,8]. Moreover, DLA aggregates grown in a d-dimensional space have a fractal dimension approximately given by $D_{DLA}\simeq(d^2+1)/(d+1)$ [9,10]. This value varies not only with the dimension d of the embedding space, but also with its topological structure; for instance, it is slightly larger for off-lattice grown aggregates and slightly smaller for aggregates simulated on square or cubic lattices [11] (although this effect is only observable for very large aggregates).

On the other hand, for $\mathrm{Pe}\to\infty$ (negligible diffusion), the ballistic deposition model applies [12], the deposits being compact and having a rough interface. The inner structure of these deposits is well described as a fat fractal, with pores distributed according to a power law [10]. Also, the interface is a self-affine fractal [10,13]. The interfacial width, defined

as the interface roughness characteristic length [see Eq. (9) below for the definition used in this paper], evolves with time according to a Family-Viksec scaling [13–15]

$$w \sim t^{\beta} f\left(\frac{t^{1/z}}{L}\right), \tag{4}$$

where $f(x)$ is a function such that $f(x \ll 1) \sim 1$, whereas $f(x \gg 1) \sim x^{-\alpha}$. The saturation effect described by $f(x)$ can be explained by the propagation of the horizontal correlation length $\xi_{\parallel}$ according to $\xi_{\parallel} \sim t^{1/z}$ while limited by the system size L. The exponent α (roughness exponent) is expressed in terms of the exponents β (growth exponent) and z (dynamic exponent) as $\alpha = \beta z$, which is derived from the existence of a steady limiting value of w for long times, induced by finite-size effects (finite value of L).

The ballistic model is considered [12] to belong to the KPZ universality [16] (with $\beta_{KPZ}=0.33$ and $\alpha_{KPZ}=0.5$ for $d=1+1$—i.e., deposition on a line—and $\beta_{KPZ}=0.25$ and $\alpha_{KPZ}=0.33$ for $d=2+1$—i.e., deposition on a surface). Several other ballisticlike models can be found in the literature which show how robust this universal KPZ behavior is when variants of the ballistic model (with modified deposition flux, particle relaxation via surface diffusion, or mixture of sticking and non sticking particles [17,18]) are considered. All these models keep the assumption of nearest neighbor transition rules, growth being led by local interactions. The presence of a diffusive component in the motion of the depositing particles, as described in the previous paragraphs, raises the question of wether this diffusive "disturbance" would keep the universal KPZ behavior.

The relationship between the particle phoretic mechanism (Pe number) and the properties of the formed deposit (interface, density, pores distribution) has been already pointed out, in the context of filter cake formation, using Monte Carlo simulations with off-lattice [5] and on-lattice methods [6]. Continuum (off-lattice) simulations are computationally expensive (due to the intrinsic nonlocality of the rules), and some properties are cumbersome to define (for instance, pores, interface). Moreover, the simulation intrinsic geometrical complexity forbids the use of large numbers of particles, thus being limited by finite-lattice-size effects. On-lattice simulations are easier to implement and faster to run, but they are not so realistic as the former ones (they have, for example, limited coordination number). However, some morphological properties that characterize large scale features (like the ones studied in [5,6,19] and in this paper) are kept, at least qualitatively, through the space-time discretization process [20].

Recently, lattice-Boltzmann methods have been used to simulate particle deposit formation on filter fibers, taking into account locally induced inhomogenities of the flow field [19]. However, this approach is not necessary when considering more uniform motions, like the one described here, where convection due to the fluid is negligible (case of phoretic forces inside a Brownian boundary layer [6]) or can be accounted for as a uniform contribution to V (as is the case in the context of filter soot cake formation, studied in Ref. [21]).

Some of the previous works were aimed at determining the effects of the deposit on the flow [19,21]. However, in other cases, the interest may be focused on bulk structure (e.g., fabrication of optical wave guides or coating by means of vapor deposition) or its adhesion or chemical interaction with the wall (fouling and corrosion in, for instance, heat exchangers) or the microscopic structure of the interface of the deposited material (e.g., catalyst [22]; see also [23] for an analogy between this sort of deposition models and particle inhalation and its inflamatory effects on the respiratory function). The study of the deposit mean features requires an statistical (micro)geometrical description of the deposition process, as used in fractal characterization.

The objective of this paper is to introduce a general method to perform discrete on-lattice Monte Carlo simulations of small particle motion and deposition with the assumptions described before and to study the relationship between the deposition mechanism (specified by the Pe number) and the relevant characteristics of the deposit bulk (described by the mean and local densities) and interface (described by its correlation lengths). Compact numerical expressions will be sought for from the simulation results in order to identify the principal mechanisms involved in deposit structure formation.

II. METHODS

The method employed in this paper is an on-lattice dynamical Monte Carlo simulation, similar to those used in [5–7]. Time will be discretized into fundamental time intervals τ. The space will be also divided in cubic cells of side $a=1$ (this will be taken as the characteristic length for the definition of Pe). Each cell can hold either fluid (empty cell) or one particle (filled cell); therefore, a is also the characteristic particle size. The bottom boundary of this lattice represents the wall where the particles deposit. At a given upper level the particles are being introduced at random locations and their trajectories being tracked down until they either reach the growing deposit or they move far away and are considered blown by the stream.

The particle motion is simulated using a dynamical Monte Carlo scheme. During a time interval τ the particle will undergo two consecutive stages: a ballistic stage and a diffusive stage [Fig. 1(a)]. During the ballistic stage, the particle jumps once in the direction pointed to by the mean deterministic velocity ("downwards"). Moreover, during the diffusive stage, the particle performs n random walk steps, n being a positive or null integer which depends on the Peclet number Pe. This scheme is chosen to ensure the isotropy of the particle diffusion in the lattice. Previous analyses which involved convection [5,6] did not fulfill this requirement and may lead to spurious effects on deposit formation. A Monte Carlo simulation with a single step is not possible for all ranges of the Peclet number (as we shall see in Sec. IV). The combination of a nonvanishing mean particle velocity and a random walk (with isotropic diffusion) requires the use of different probabilities of particle jumps on the different lattice directions. For some values of the Peclet number, the one-step Monte Carlo model leads to a negative probability

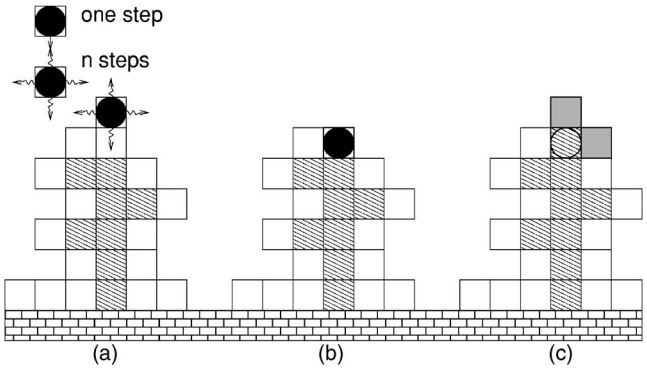

FIG. 1. Particle motion and deposition model over a wall (at the bottom). Particle moves applying two alternating rules (mean velocity and difussion): a deterministic jump towards the wall, followed by n random walks (a). The particle moves until it reaches a cell labeled as active [open squares in (b)]; the particle sticks there and marks this cell as occupied and every empty nonactive neighbor cell as a new active cell [solid grey cells in (c)].

for particle jumps in the direction opposed to the mean flow. The use of the two-stage Monte Carlo model, with a ballistic step followed by n random steps, avoids the existence of negative probabilities while ensuring the isotropy in the particle diffusion.

According to the definition of the first stage, the mean particle velocity relates the time and space discretizations by $V=a/\tau$. Hence the value of the fundamental time interval τ is fixed by the Monte Carlo scheme.

To determine n, we consider that for a random walker in a d-dimensional space (i.e., a particle that may jump from its cell to any of its neighbors with equal probability p_D or stay at its current location with probability $1-2dp_D$) the position variance after n steps becomes

$$(2dp_D)na^2 = 2d\mathcal{D}\tau, \tag{5}$$

which is the Einstein's relation linking particle position variance to time τ and diffusion coefficient $\mathcal{D}$. Substituting in Eq. (5) the expression (3) for the Peclet number, the value $n=(p_D\mathrm{Pe})^{-1}$ is obtained. Obviously, the use of this relation with a maximum symmetric jump probability $p_D=1/2d$ will restrict the simulation to values of the Peclet number which provide an integer value of n. To overcome this difficulty, a nonjump probability p_0 has to be introduced. In this way n can be fixed and p_D evaluated afterwards. Let us take

$$n = \mathrm{int}\left(\frac{2d}{\mathrm{Pe}} + 1\right) \tag{6}$$

[by int(x) we denote the integer part of x]. Then we get for the jump probability (the same for every neighbor cell irrespectively of the orientation of the mean particle velocity)

$$p_D = \frac{1}{n\mathrm{Pe}} < \frac{1}{2d},$$

thus remaining a nonjump probability (probability of remaining at the same position)

$$p_0 = 1 - 2dp_D > 0$$

in each of the n random walk steps of the diffusive stage.

Particle motion starts at the level "one cell over the topmost particle in the deposit" but at a random horizontal location. The number of diffusive jumps in the first Monte Carlo step (the first τ seconds) of every particle motion is chosen at random between zero and the maximum number of diffusive jumps, n, for the simulated Peclet number, given by Eq. (6). The motion of a particle ends when it "touches" the surface of the wall or the deposit [Fig. 1(b)]. To avoid seeking the state of all nearest-neighbor cells, the active site bookkeeping algorithm is used [7]. A particle motion is then stopped whenever it enters an active cell; this cell will become filled and all of its empty neighbors labeled as new active cells [solid grey cells in Fig. 1(c)].

It is known that, as the deposit grows, long-range correlations propagate through its interface. This is responsible for the appearance and propagation of border effects when the surface is considered bounded, and free or nonfree conditions are assumed on those boundaries. It is also responsible for the modification (increase and saturation) of the roughness when measured over small regions of the interface (this effect leads to the Family-Viksec scaling ansatz [14]). To avoid the first effect and to decrease the latter, periodic boundary conditions are assumed along the directions parallel to the wall and the lattice base size L is chosen large compared to the maximum height correlations which may appear during the deposit evolution.

Computer experiments

The two-stage Monte Carlo scheme just described is used for three-dimensional (3D) simulations on a cubic lattice with square bases of side $L=400a$ (for the bulk characterization) and $L=512a$ (for the interface characterization) and periodic lateral boundary conditions. The range of Pe numbers considered varies from 0.1 to 1000. Values will be taken to be logarithmically spaced to have representative sampling of the parameter space (deposit structure varies slowlier with Pe the larger the Peclet number is).

To estimate the reproducibility of the numerical results we compute standard deviations over 10 (for the bulk characteristics) or 30 (for the interface) individual simulations. For those parameters obtained by regression, standard errors will be used as uncertainty estimations.

III. RESULTS

The structure of the deposits has been characterized numerically by macroscopic properties of their surface and bulk: *bulk density*, both *average* and *microscopic*, and *interfacial correlations*, both *horizontal and vertical* (i.e., *growth interface width*).

A. Density

The simplest way to characterize the bulk of a deposit is through its density profile [5]. For a given time, the density

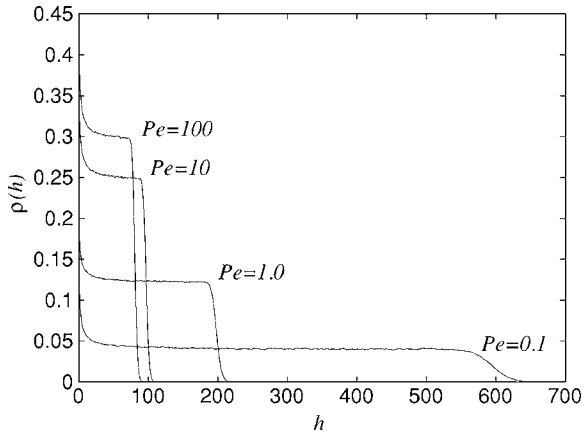

FIG. 2. Deposit density, ρ, vs. height, h, for $Pe=0.1$, 1.0, 10, 100, for deposits of 5×10^6 particles.

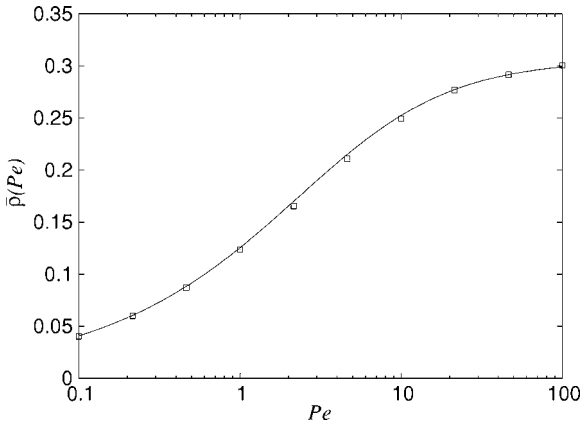

FIG. 3. Plateau density dependence on the Peclet number $\bar{\rho}(\mathrm{Pe})$. Squares represent the values obtained from averages over ten simulations; error bars are not shown (relative errors remain smaller than 10^{-3}). The line corresponds to the fitting expression (7).

profile $\rho(h)$ is the function representing the fraction of occupied cells at a given height h,

$$\rho(h) = \frac{N(h)}{L^2},$$

where $N(h)$ is the number of deposited particles at height h over the wall. Some density profiles are shown in Fig. 2.

This density depends on the height inside the deposit h as well as on the Peclet number Pe. It is higher near the wall, decreases to a plateau value $\bar{\rho}$ for intermediate heights, and then decreases to zero in the upper areas where new particles are still arriving (the *active zone*). The existence of the plateau [5,6] is due to the fact that, some time after deposition begins (earlier the higher the Pe is), a part of the deposit becomes "frozen" so that no more particles penetrate that region which remains with a fixed density $\bar{\rho}$.

The initial deposition stages (thus, lower heights) are affected by the presence of the rigid wall and a higher deposit density is reached there. This initial boundary effect is generally observed in deposition and growth experiments as those recently illustrated by Yu *et al.* [24] using scanning electron microscope (SEM) images. Quoting these authors, the porous structure is due to the penetration of the arriving particles through the pores of the deposit, which gives a uniform density (the "plateau" in our simulations) which depends on the preferential landing of the particles (the diffusive component in our model enhances deposition on the tips). When the substrate is not the porous deposit, this penetration is not possible and the particles form a more compact structure as is seen in the microphotographs of Yu *et al.* and in the lower parts of our simulations. Beyond the initial influence of the wall a constant value of $\bar{\rho}$ is attained which is characteristic of the deposit growth mechanism.

In the plateau region $\bar{\rho}(Pe)$ is an increasing function of Pe, going from very low values in the diffusion-dominated particle deposition limit $\sim$0.05 for Pe=0.1, to a maximum value of about 0.3 for pure ballistic particle deposition (Pe $\to\infty$). We find (see Fig. 3) that it is possible to fit $\bar{\rho}(\mathrm{Pe})$ to the expression

$$\bar{\rho}(Pe) = \bar{\rho}(\infty)\left[1 + \frac{A_\rho}{\mathrm{Pe}}\right]^{-D}, \tag{7}$$

with $A_\rho \simeq 4.8$ and $D \simeq 0.52$, with $\bar{\rho}(\infty) \simeq 0.302$, the value of $\bar{\rho}(\mathrm{Pe}\to\infty)$, corresponding to a ballistic deposit mean density (all decimal figures are significative within the fitting interval, giving values which differ from the numerical simulation averages in less than 1%).

Expression (7) for $\bar{\rho}(\mathrm{Pe})$ becomes zero as $\mathrm{Pe}\to 0$. This is expected from the DLA limit of our model, because for a vanishing Peclet number, the deposit structure becomes fractal (whose average density is zero). However, due to finite-size effects of the simulations, this zero-limit average density will not be reached. Instead the density of the plateau region achieves a minimum value which decreases as the deposit horizontal length (L) increases. We have taken this into account and checked (comparing the results from smaller and larger lattices) that, for the range of Peclet numbers simulated, these effects are unimportant. In the discussion (Sec. IV) we will give a criterium to find the minimum lattice size which allows to simulate the inner structure of a deposit in terms of the Peclet number describing the motion of the particles used to grow it.

B. Local density scaling

To characterize the inner structure of the deposit, a box-counting approach was used to study the scaling of the "local density" $\bar{\rho}(\ell)$, defined as the mean mass-to-volume ratio in a box of size ℓ:

$$\bar{\rho}(\ell) \sim \left\langle \frac{\text{mass within a box of size } \ell}{\text{volume of a box of size } \ell} \right\rangle.$$

Here the average corresponds to positions inside the frozen region of the deposit (the "plateau," in the density profile plot). We compute the number of boxes of a given size ℓ needed to cover all the particles in that region of the deposit and then the mean particle density in these boxes. Due to box size discretization, some boxes will be only partially within

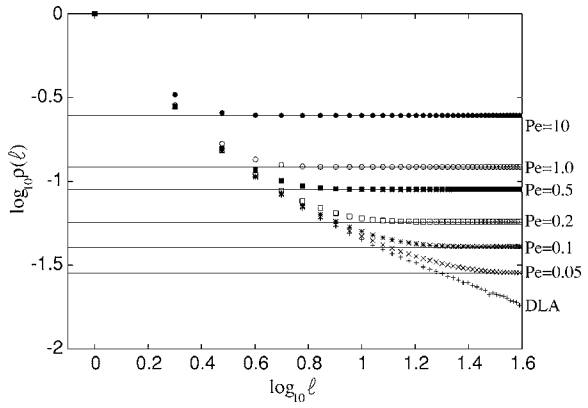

FIG. 4. $\log \bar{\rho}(\ell, \mathrm{Pe})$ vs $\log \ell$, for Pe=0.05, 0.1, 0.2, 0.5, 1.0, 10. Horizontal lines represent the asymptotic mean density, as given by Eq. (7). Also shown are the results of applying the same box-counting method to a DLA aggregate grown inside a $400\times400\times400$ box.

the region of study (the "plateau")—i.e., only N_ℓ of their ℓ^3 cells will be inside the studied region. To achieve smoother results, these boxes will be counted with a weight of N_ℓ/ℓ^3.

All box-counting plots show an initial common region for small values of ℓ (visible for $\mathrm{Pe}<1$) in which their scaling behavior looks the same as that observed for DLA clusters (seen in Fig. 4). For larger box sizes (larger the smaller the Peclet) the local density saturates to the mean deposit density.

C. Interface width

Deposit interface can be characterized by the statistical description of the active region (the interface where growth is taking place at a given moment). This is usually done (see [10,12,13]) in an operational way, by giving the mean height of newly deposited ballistic particles (i.e., with $\mathrm{Pe}\to\infty$), which corresponds to the average height $\bar{h}$ of the topmost *active sites* over each of the L^2 lattice square base sites,

$$\bar{h} = \frac{1}{L^2}\sum_i^{L\times L} h_i, \tag{8}$$

and the interface width which is taken as the typical deviation of the ballistic probe particle arrival heights w also computed from the topmost active site distribution:

$$w^2 = \frac{1}{L^2}\sum_i (h_i - \bar{h})^2. \tag{9}$$

A generalization of this approach is to define a Peclet-dependent mean height and width computed using probe particles whose motion is the same as that of the depositing particles building up the deposit. We will denote these quantities $\bar{h}_{Pe}$ and w_{Pe}, respectively, with a subscript Pe to emphasize that they are computed using probe particles moving according to the algorithm just described at the beginning of this section, for the given Peclet number.

To describe horizontal correlations for an interface defined by the height function $h(\mathbf{x})$, a correlation length $\xi_{\|Pe}$ can be computed [15] based on the height-height correlation function

$$\Gamma_{h,Pe}(\mathbf{x}) = \langle [h_{Pe}(\mathbf{x}^0) - \bar{h}_{Pe}][h_{Pe}(\mathbf{x}^0+\mathbf{x}) - \bar{h}_{Pe}]\rangle_{\mathbf{x}^0},$$

where the product is averaged over the horizontal coordinates $\mathbf{x}_0$ of the reference points. We will use as $\xi_{\|Pe}$ the mean decay length of $\Gamma_{h,Pe}(\mathbf{x})$ given by [15]

$$\xi_{\|Pe} = \frac{\int \Gamma_{h,Pe}(x)x\,dx}{\int \Gamma_{h,Pe}(x)\,dx}.$$

The evaluation of $\xi_{\|Pe}$ will be carried out using a Monte Carlo sampling of points, as for w_{Pe}.

In the following we present results describing the long-time (i.e. scaling behavior) evolution of the active region interface. To describe the temporal evolution of $\xi_{\|Pe}$ and w_{Pe}, we have taken as natural time the unit $T_{L\times L}$, the inverse of the particle arrival rate per unit surface, given in terms of the particle flux density normal to the wall, $\mathbf{j}_w\cdot\mathbf{n}$, and by the average projected area of a particle, a^2, as $T_{L\times L} = (\mathbf{j}_w\cdot\mathbf{n}a^2)^{-1}$.

The true value of this time unit depends on the value of $\mathbf{j}_w$ determined by the fluid dynamics solution of the particle distribution in the flow field surrounding the deposition wall. That solution can be computed as in [3] with the usual boundary conditions for the flow velocity at the wall and assuming there a perfectly absorbing boundary for the particle concentration. In our simulations, $T_{L\times L}$ corresponds to the time needed to deposit as many particles as cells are in the lattice base—i.e., L^2 (hence the notation). This allows us to use a lattice-size-independent time t, while the physical time can be recovered as $tT_{L\times L}$.

D. Horizontal correlations

The horizontal correlation length $\xi_{\|Pe}$ shows a small initial transient. When $\xi_{\|Pe}$ becomes large enough (larger than $4a$) a power-law region begins,

$$\xi_{\|Pe} = A_\xi t^{1/z}, \tag{10}$$

spanning a variable-time interval (up to values of $\xi_{\|Pe}$ around $30a$). We will use this range as the fitting region to estimate the growth exponents. Later on, $\xi_{\|Pe}$ starts to oscillate due to increasing sample variability and saturation.

This exponent z^{-1} is analogous to that appearing in the expression of the Family-Vicsek scaling ansatz (4) although its saturation effects are not yet observable in our simulations. Some plots used for its estimation are shown in Fig. 5 and some estimates are recorded in Table I and represented in Fig. 9, below, for several Pe values.

E. Long-time w_{Pe} evolution

For long times, after a short initial transient, a power-law behavior for w_{Pe} is observed,

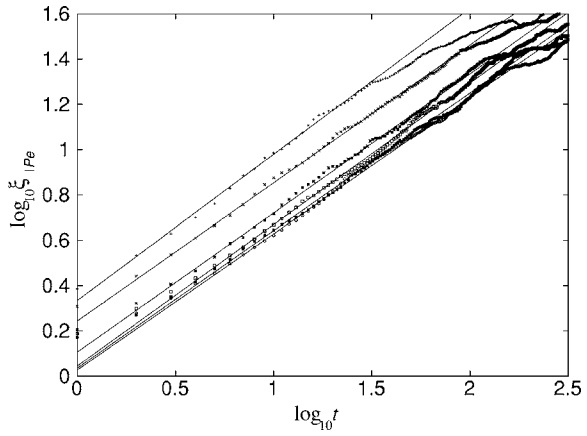

FIG. 5. Long-time horizontal correlation length $\xi_{\|Pe}$ evolution for Pe=0.5, 1, 5, 10, 100, 1000. Shown as solid lines are the fittings to expression (10).

$$w_{Pe} = A_w t^{\beta}, \tag{11}$$

with the exponent β varying from 0.220 ± 0.003 for Pe $=1000$ to about 0.272 ± 0.005 for Pe$=0.5$. Regressions were performed within the region where $4 < \xi_{\|Pe} < 30$, as in the previous case. The exponent β corresponds to the initial power-law growth described by expression (4). Some plots used for its estimation, corresponding to different Peclet numbers, are shown in Fig. 6 and the obtained values are given in Table I and plotted in Fig. 9, below.

F. Self-affine characterization

To characterize the vertical to horizontal correlation dependence of the active region, w_{Pe} was represented against $\xi_{\|Pe}$. A power law was obtained, in the form

$$w_{Pe} \propto \xi_{\|Pe}^{\alpha}, \tag{12}$$

with the exponent α varying from 0.366 ± 0.012 for Pe$=20$, to about 0.415 ± 0.017 for Pe$=0.5$. Regressions were performed within the region $4 < \xi_{\|Pe} < 30$, as before. Some plots used for the estimation of α are shown in Fig. 7. Moreover the exponent α is given in Table I and also in Figure 9, below, for several values of the Peclet number Pe.

TABLE I. Long-time scaling exponents for several Peclet numbers α (roughness exponent), β (growth exponent), and z (dynamic exponent).

Pe	α	β	z^{-1}	z
0.5	0.415 ± 0.017	0.272 ± 0.005	0.655 ± 0.018	1.53
1.0	0.409 ± 0.012	0.249 ± 0.005	0.616 ± 0.018	1.62
5.0	0.403 ± 0.015	0.251 ± 0.005	0.622 ± 0.023	1.61
10	0.385 ± 0.013	0.242 ± 0.004	0.624 ± 0.017	1.60
100	0.371 ± 0.015	0.223 ± 0.005	0.600 ± 0.019	1.67
1000	0.370 ± 0.009	0.220 ± 0.004	0.602 ± 0.016	1.66

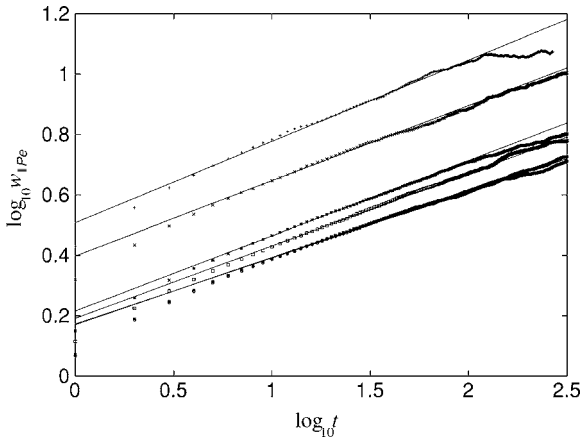

FIG. 6. Long-time active region width w_{Pe} evolution for Pe $=0.5$, 1, 5, 10, 100, 1000. Shown as solid lines are the fittings to relation (11).

IV. DISCUSSION

In previous works [23,25] a single stage Monte Carlo model (directly inspired in [6]) was used. There, the jump probabilities $p_{\pm i}$ (i corresponds to the direction and a + or − sign indicates forward or backward jump; deterministic velocity is assumed along the "$-z$" direction) were assigned subject to the conditions

$$p_{+i} - p_{-i} = p_D \mathrm{Pe} \mu_i,$$

$$p_{+i} + p_{-i} = p_D (2 + p_D Pe^2 \mu_i^2),$$

$$\sum_i (p_{+i} + p_{-i}) = 1,$$

with p_D given by Eq. (5) assuming $n=1$, $\mu_i=-1$ for i perpendicular, and $\mu_i=0$ for i parallel to the depositing substrate. This model introduces different probabilities in the two senses along the direction defined by the mean particle velocity to ensure an isotropic particle diffusion. However, it

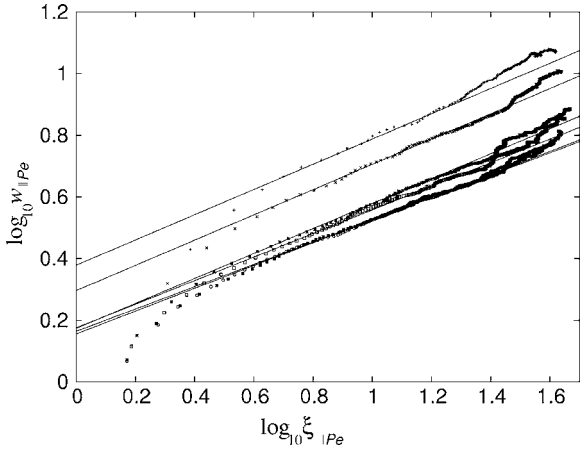

FIG. 7. Active region width vs horizontal correlation length for Pe$=0.5$, 1, 5, 10, 100, 1000. Solid lines correspond to expression (12).

has the drawback of being valid only for $\mathrm{Pe} < \mathrm{Pe}_{\max} = 2(d-1)/(d-2)$. Above this $\mathrm{Pe}_{\max}$ ($\mathrm{Pe}_{\max}=4$ for 3D simulations), an unphysical negative value is obtained for the ascending probability. To avoid the use of a negative probability, the conditions for the random numbers generated in the simulation were evaluated first in those directions where no negative probabilities arose and then along the falling direction [25].

The results presented in this work coincide (within statistical error bars) with those obtained with the previous model not only within its region of applicability, but also for $\mathrm{Pe} > 4$. The reason is that, for high Peclet number, the main contribution is ballistic, and ascending probability can be neglected; it can be assumed that, whenever a vertical jump happens, it will be descending with probability $p_+ = 1 - 2(d-1)p_D$.

Anyway, the two-stage Monte Carlo simulation used here (with a deterministic step and n random walk steps) eliminates this negative probability and avoids the appearance of spurious effects for large-Peclet-number simulations.

The characteristic density of the deposit, given by Eq. (7), reproduces a power law for low values of Pe (as was noted in [6] through the measurement of the mean height $\bar{h}$). The prefactor $\bar{\rho}(\infty)$ corresponds to the density of a purelly ballistic deposit, $\bar{\rho}(\mathrm{Pe} \to \infty) \simeq 0.302$, and the exponent of the power law is $D = 0.52$. Moreover, the coefficient A_ρ is of order unity ($A_\rho \simeq 4.8$) and represents the crossover Peclet number between power-law behavior and ballistic saturation. As was pointed out in [25] (where an analogous result was observed for 2D simulations) D is numerically close to $d - D_{DLA}$, d being the dimension of the space and D_{DLA} the fractal dimension of a DLA aggregate.

To explain this numerical coincidence, we rescale the time-independent version of Eq. (2) with a characteristic length $l \times a$,

$$\partial_z c + \frac{1}{l} Pe^{-1} \nabla^2 c = 0$$

(here, l does not need to be an integer). This expression describes the quasistationary distribution of particles near the deposit interface. We observe that, for scales where $\mathrm{Pe}^{-1}/l \gg 1$, the diffusive term becomes dominant, while for $\mathrm{Pe}^{-1}/l \ll 1$, it is negligible. There must exist a length scale $l_0 a$, given by the condition $l_0 \sim \mathrm{Pe}^{-1}$, such that the particle behavior can be considered diffusive for scales below l_0 (and fractal structures should arise at those scales) and ballistic for the scales above (and correspondingly, structures will be compact).

Therefore, the numerical correlation given by Eq. (7) can be interpreted as a Pe limitation to the size of DLA-like structures that produces a mean density similar to that of "small DLA fractals" of size $(1 + A_\rho/\mathrm{Pe}) \times a$ (here we have added a length a to ensure a minimum aggregate size of one cell).

An argument similar to this was already proposed by Meaking [26] in the context of DLA growth with biased probabilities.

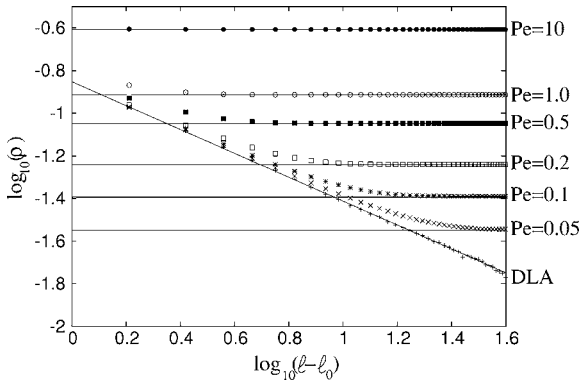

FIG. 8. log-log plot (base 10) of $\bar{\rho}(\ell, \mathrm{Pe})$ vs ℓ, showing the gradual departure from the DLA power law [Eq. (13), shown as the oblique line] for increasing Pe=0.05, 0.1, 0.2, 0.5, 1.0, 10.

In order to check this local fractality model, the results in Sec. III B can be used to find a fractal dimension of the deposit bulk through the usual box-counting algorithm.

First of all, we seek a power-law expression fitting the values obtained for small boxes—that is, in the common scaling region. The power-law behavior of the box-counting plot is expected to hold in a range of box sizes large compared to one cell (and small compared to the deposit size). Therefore we will need to use a modified expression to recover a power law for the small boxes we are interested in. To obtain a power law for a DLA fractal box counting using boxes with fewer than $10 \times 10 \times 10$ cells, the following "corrected" expression may be used:

$$\bar{\rho}(\ell) = \rho_1 \times (\ell - \ell_0)^{-D}, \tag{13}$$

where $\rho_1 \simeq 0.140 \pm 0.005$, $D = -0.560 \pm 0.005$, and $\ell_0 = 2.37 \pm 0.06$ is taken so that fitting residual rms, for $4 < \ell < 40$, is minimum (this implies neglecting measures with boxes smaller than three cells wide). The value of ρ_1 represents the power prefactor extrapolated from the large-box behavior—that is, from the region where the power law does not depend on ℓ_0. The exponent $D = D_{DLA} - d$ gives the estimate $D_{DLA} \simeq 2.44$.

Deposits grown with $\mathrm{Pe} < 1$ follow approximately the same power law, until the density given by Eq. (7) is attained (shown in Fig. 8). Therefore, particle deposits are DLA-like fractals up to a scale $\sim 1 + A_\rho/\mathrm{Pe}$ and simply porous above that scale.

This local fractality interpretation is useful when choosing the size of a simulation in order to avoid finite-size effects in the estimation of, for example, the plateau density. The minimum Pe that could be reliably simulated in a box of size L would be $\mathrm{Pe}_{\min} = A_\rho/(L-1)$; for our simulations where $L = 400a$, $\mathrm{Pe}_{\min} \simeq 0.012$. For lower values of Pe, the measured density will be higher than predicted by Eq. (7) and it will show a stronger dependence on L than on the Peclet number.

The power-law exponent of -0.56 does not concide exactly with that expected from the mean density fitting, -0.52. This discrepancy probably means that other limiting effects

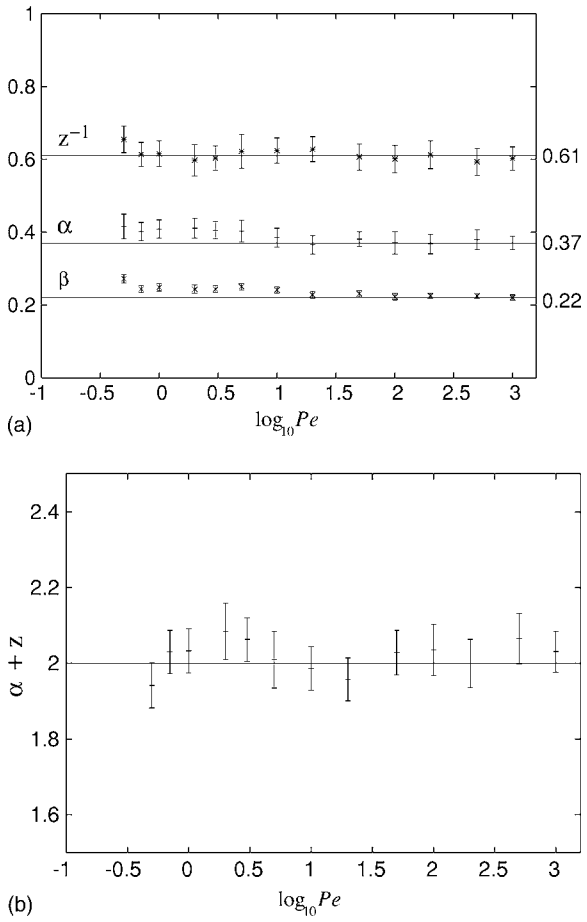

FIG. 9. (a) Long-time growth exponents α, β, and z^{-1} versus Peclet number. (b) Value of $\alpha+z$ as a function of Peclet number.

apart from the convective ones accounted for in our heuristic model need to be considered.

For $\mathrm{Pe}>1$, no initial power-law region can be resolved using this box-counting procedure because we have neglected very small boxes in order to get better fit in a wider power-law region. However, it can be seen from the average densities that Eq. (7) is still valid, suggesting that the same mechanism is still operating.

The active region scaling is described by the exponents α, β, and z appearing in expressions (4) and (10)–(12) computed from the results shown in Figs. 5–7. Some values of these exponents are quoted in Table I and summarized in Fig. 9. We have employed in this paper the usual notation for the dynamic exponent z; however, we give the value of z^{-1} because this is the exponent directly computed from the fitting to expression (10).

Due to the small number of simulations (30 for each Peclet number), 10%-trimmed averages have been used to discard outliers (values far from the average). Standard errors have been obtained through a bootstrap method with 1000 subsamples [27].

The exponent β was estimated by means of linear regression for each Peclet number after averaging the time evolution of w_{Pe} over 30 simulations. The regularity observed suggests a characteristic value around 0.24 ± 0.02. In fact, it falls between the ballistic deposition exponent $\beta_{BD}\simeq0.22$ of [28] and the KPZ exponent $\beta_{KPZ}=0.24$ estimated in [29]. The former value β_{BD} is closer to those values of β obtained for $\mathrm{Pe}>10$, while for $\mathrm{Pe}<10$, the value of β becomes closer to β_{KPZ} [see Fig. 9(a)].

The exponent z^{-1} was estimated in a similar manner. A characteristic value of $z^{-1}=0.61\pm0.02$ is achieved. This value differs only slightly from the KPZ expected value of $z_{KPZ}^{-1}=0.625$.

From the w_{Pe} vs $\xi_{\|Pe}$ plot, the roughness exponent α can be estimated. The characteristic value is $\alpha=0.38\pm0.02$ which can also be obtained from the relation $\alpha=\beta/z^{-1}$ using the previous results for β and z^{-1}. As happened for β, the α estimates for $\mathrm{Pe}>10$ fall nearer the ballistic deposition result of 0.366 reported by Aarao Reis in [30] from large ballistic deposition simulations. For $\mathrm{Pe}<10$, the estimated value of α is closer to 0.4, which is the KPZ limit reported by [29]. As can be seen in Fig. 9(b), the relation $\alpha+z=2$, characteristic of KPZ universality, is approximately fulfilled.

From the previous considerations we can say that, within the range of Peclet number values explored (that is, for $\mathrm{Pe}>0.5$), the growth interface scales as KPZ or, at least, it is within its basin of attraction as happens for pure ballistic deposition.

V. CONCLUSIONS

We have introduced a Monte Carlo model for the on-lattice simulation of particle motion in the presence of convection and diffusion which keeps diffusion coefficient isotropic. We have used this model in simulations for the growth of particle deposits over a planar surface in the presence of a convective velocity towards the surface and including the diffusive behavior of the arriving particles. The relative importance of the deterministic velocity to the diffusive transport is measured by the Peclet number.

The numerically obtained macroscopic deposit properties depend on the Peclet number in a way well described by numerical correlations for the deposit characteristic density (7), local density scaling (13), and the long-time evolution of the surface active region—that is, the region where growth takes place effectively [Eqs. (10)–(12)].

To explain the obtained expressions a heuristic model of local DLA fractal growth was presented. This heuristic model is compatible with the observed local density scaling.

The interfacial region has been shown to have a self-affine scaling of KPZ type, with small influence of the DLA-like growth or the Peclet number.

Thus, the presented model relates deposit microstructure to transport mechanisms. It shows how to use transport parameter variation (namely, the Peclet number) to tune the porosity and roughness (and, hence, active surface) of the deposit, while keeping the local bulk and interface fractal structures between those produced by diffusive processes—i.e., DLA like—and the overall self-affine KPZ scaling.

The numerical correlations presented in this paper will be helpful in the description of experimentally obtained particle deposits under the general assumptions presented in the Introduction. Although some of the coefficients given will have

to be fitted to the observed data [for instance, ρ_∞ in Eq. (7)], the link between functional dependences and the microscopic description of the structure could be helpful when microscopic characterization techniques are limited. Also, the failure of the presented correlations to describe the experimental situations would indicate that some other effects (e.g., sintering or relaxation) are becoming relevant and should be included in the model.

ACKNOWLEDGMENTS

The authors would like to thank Dr. Pedro Cordoba (UNED) for enlightening conversations and suggestions about the characterization of interfacial roughening.

This work has been supported by DGI, Ministry of Science and Technology, Spain, under Project Nos. DPI 2002-04550 and DPI 2005-04601.

[1] N. A. Fuchs, *The Mechanics of Aerosols*, 1st ed. (Dover, New York, 1981).
[2] S. K. Friedlander, *Smoke, Dust, and Haze: Fundamentals of Aerosol Dynamics*, 2nd ed. (Oxford University Press, Oxford, 2000).
[3] P. L. Garcia-Ybarra and J. L. Castillo, J. Fluid Mech. **336**, 379 (1997).
[4] J. L. Castillo, P. L. Garcia-Ybarra, and A. Perea, J. Aerosol Sci. **32**, S939 (2001).
[5] D. Hui and R. Lenormand, in *Kinetics of Aggregation and Gelation*, edited by F. Family and D. P. Landau (Elsevier Science, New York, 1984).
[6] M. Tassopoulos, J. A. O'Brien, and D. E. Rosner, AIChE J. **35**, 967 (1989).
[7] T. A. Witten and L. M. Sander, Phys. Rev. Lett. **47**, 1400 (1981).
[8] P. Meakin, Phys. Rev. A **27**, 2616 (1983).
[9] M. Muthukumar, Phys. Rev. Lett. **50**, 839 (1983).
[10] T. Viksec, *Fractal Growth Phenomena* (World Scientific, Singapore, 1989).
[11] S. Tolman and P. Meakin, Phys. Rev. A **40**, 428 (1989).
[12] P. Meakin, P. Ramanlal, L. M. Sander, and R. C. Ball, Phys. Rev. A **34**, 5091 (1986).
[13] A. L. Barábasi and H. E. Stanley, *Fractal Concepts in Surface Growth*, 1st ed. (Cambridge University Press, Cambridge, England, 1995).
[14] F. Family and T. Viksec, J. Phys. A **18**, L75 (1985).
[15] J-F. Gouyet, M. Rosso, and B. Sapoval, in *Fractals and Disordered Systems*, edited by A. Bunde and S. Havlin (Springer-Verlag, Berlin, 1991), pp. 264–301.
[16] M. Kardar, G. Parisi, and Y-Ch. Zhang, Phys. Rev. Lett. **56**, 889 (1986).
[17] R. Baiod, D. Kessler, P. Ramanlal, L. M. Sander, and R. Savit, Phys. Rev. A **38**, 3672 (1988).
[18] Y. P. Pellegrini and R. Jullien, Phys. Rev. A **43**, 920 (1991).
[19] R. Przekop, A. Moskal, and L. Gradoń, J. Aerosol Sci. **34**, 133 (2003).
[20] P. Meakin, Phys. Rev. A **27**, 1495 (1983).
[21] A. G. Konstandopoulos, E. Skaperdas, and M. Masoudi (unpublished).
[22] M.-O. Coppens, Catal. Today **53**, 225 (1999).
[23] D. Rodríguez-Pérez, J. L. Castillo, and J. C. Antoranz, in *Computational Methods in Neural Modelling*, edited by J. Mira and J. R. Alvarez (Springer, Berlin, 2003), pp. 366–373.
[24] Y. Yu, J. L. Shui, S. Xie, and C. H. Chen, J. Aerosol Sci. **39**, 276 (2005).
[25] D. Rodríguez-Pérez, J. L. Castillo, and J. C. Antoranz, J. Aerosol Sci. **34**, S509 (2003).
[26] P. Meakin, Phys. Rev. B **28**, 5221 (1983).
[27] B. Efron, *The Jackknife, the Bootstrap and Other Resampling Plans*, 1st ed. (Society for Industrial and Applied Mathematics, Philadelphia, 1990).
[28] J. Kertész and T. Vicsek, in *Fractals in Science*, edited by A. Bunde and S. Havlin (Springer, Berlin, 1995), pp. 88–117.
[29] E. Marinari, A. Pagnani, and G. Parisi, J. Phys. A **33**, 8181 (2000).
[30] F. D. A. Aarao Reis, Phys. Rev. E **63**, 056116 (2001).